JOURNAL OF GEOPHYSICAL RESEARCH, VOL. 105, NO. A3, PAGES 5517–5528, MARCH 1, 2000

Solar wind control of the tail lobe magnetic field as deduced from Geotail, AMPTE/IRM, and ISEE 2 data

N. A. Tsyganenko [1]

Laboratory for Extraterrestrial Physics, NASA Goddard Space Flight Center, Greenbelt, Maryland

Abstract. A statistical study was made of the tail lobe field response to the dynamical pressure of the incoming solar wind and to the interplanetary magnetic field, as well as its relation to the concurrent level of the *Dst* field. The study covers a wide range of distances between 10 and $60R_E$ and is based on a large set of tail lobe magnetic field data, compiled from three sources: (1) Geotail magnetometer and low-energy plasma instrument data for 1993-1997, (2) AMPTE/IRM magnetometer and plasma instrument data for 1985-1986, and (3) ISEE 2 magnetometer and fast plasma experiment data for 1978-1980. The tailward variation of the tail lobe field and of its response to the solar wind and interplanetary magnetic field (IMF) conditions was studied using a regression relationship, including various combinations of the interplanetary quantities, measured by IMP 8 and Wind spacecraft. An investigation of the role of the time lag effects was made by tagging each lobe field measurement by a "trail" of 12 consecutive 5-min average values of the solar wind parameters and finding best fit distributions of the lagged response amplitudes in the solar-wind and IMF-related regression terms. The goal of the work is to find a set of input variables providing the highest correlation between the observed and predicted magnitude of the tail lobe field, so that their combination could be used for parameterizing the strength of the cross-tail current in the data-based magnetospheric models.

1. Introduction

A principal requirement on a global magnetospheric model is its ability to accurately reproduce the configuration of the magnetic field, given the data on the state of the incoming solar wind. Early models [*Mead and Fairfield*, 1975; *Tsyganenko and Usmanov*, 1982; *Tsyganenko*, 1987, 1989] did not directly use any solar wind data and parameterized the geomagnetic field only by binning the data and model coefficients into several intervals of the *Kp* index. In the more recent T96 model [*Tsyganenko*, 1995, 1996, 1998] a continuous parameterization by the solar wind pressure, interplanetary magnetic field (IMF), and the *Dst* index was adopted instead of the crude binning by the *Kp* index. A similar approach was also used by *Ostapenko and Maltsev* [1997] in an attempt to construct an improved model of the inner magnetospheric field; they used the database of *Fairfield et al.* [1994] and represented their model coefficients as linear functions of the *Dst* and *Kp* indices, the solar wind pressure, and the IMF B_z. The model of *Hilmer and Voigt* [1995] did not use any magnetospheric field data but was also parameterized by observable variables, such as the solar wind pressure, *Dst* index, and the equatorward boundary of the diffuse aurora.

A major source of the global magnetospheric field is the cross-tail current. In the T96 model the tail field was represented by a sum of two independent modules, corresponding to the near-Earth and the distant parts of the magnetotail current. The magnitude factor for each of the modules was represented as a linear function of the normalized solar wind parameters

$$a + b\left(\sqrt{P_d/\langle P_d\rangle} - 1\right) + c\,(\gamma/\langle\gamma\rangle - 1)\ , \qquad (1)$$

including the square root of the dynamic pressure of the solar wind $P_d = \rho V^2$ in the second term and the parameter γ in the third term, describing the effect of the IMF upon the tail field. More specifically, the quantity γ was defined as

$$\gamma = \sqrt{N}\,V\,B_t \sin\frac{\theta}{2} \qquad (2)$$

where N, V, B_t, and θ are the solar wind ion density, speed, IMF transverse component, and the IMF clock angle, respectively. It was found that the pressure-dependent term in (1) generally dominated over the IMF-related one, although a dramatic difference was also observed in the degree of the closure of the tail field lines across the plasma sheet between the cases of northward and southward IMF [*Tsyganenko*, 1996, 1998].

While demonstrating the general robustness and reasonable behavior of the data-based model field in response to the external factors, those results posed further questions. In particular, the form (1) is just one of many possible regression relations, and it remains unclear how far it is from the best

[1] Also at Raytheon ITSS Corporation, Lanham, Maryland.

Copyright 2000 by the American Geophysical Union.

Paper number 1999JA000375.
0148-0227/00/1999JA000375$09.00

choice. For example, one could try different powers of P_d in (1) instead of the square root dependence. Note in this regard that in a similar study by *Nakai et al.* [1991] the tail lobe field $B_{\rm lobe}$ was postulated to depend linearly on P_d. While that assumption could be justified for a relatively narrow interval of P_d, in reality the values of the solar wind pressure can vary from as low as 0.1 to 20 nPa and even higher, so that a linear relationship is unlikely to remain accurate in the entire range. In the middle and distant tail, a simple estimate based on the transverse pressure balance suggests $B_{\rm lobe} \sim \sqrt{P_d}$, assuming that the external pressure on the lobes is proportional to P_d. However, in the near tail all these approximations become questionable because as one approaches Earth, the magnetic field rapidly increases and becomes strongly nonuniform in all three dimensions. In this work, the effect of the solar wind pressure on the tail lobe field is studied in more detail, using a refined set of data taken in a wide range of distances and assuming different forms of the pressure-related term in a regression equation.

Concerning the IMF-dependent term in (1), the specific form (2) of the index γ was adopted in the T96 model solely because of its high correlation with the intensity of the field-aligned currents, reported by *Iijima and Potemra* [1982]; however, that did not necessarily mean that the index was best for parameterizing the tail current. *Nakai et al.* [1991] used a linear regression model in which the IMF dependence was represented by the term VB_z. In this work, several other IMF-related combinations of the interplanetary quantities were tried, and the best results were indeed obtained for a different control variable, as discussed in more detail below.

Another interesting problem is the delay in the response of the tail field to the IMF conditions owing to the finite time required to transfer magnetic flux from the solar wind to the tail lobes. *Nakai et al.* [1991] used hourly averages of the solar wind parameters and assumed a 1-hour lag for the quantities entering in the term VB_z. However, no detailed study of time lag effects was made so far. In the present work, the solar wind data at 5-min resolution were used, which allowed us to pay more attention to the delayed response of the tail field to the solar wind conditions.

Another way to improve the accuracy of the model is to use more control variables in the regression equation. One of possible candidates is the *Dst* index. Although it is not independent of the solar wind parameters, the *Dst* index has an advantage that it directly reflects the actual strength of the near-Earth field sources at a given time. While the largest contribution to the *Dst* field comes from the ring current, one can expect that the cross-tail current (at least, its near-Earth portion) is an important source as well [*Maltsev et al.*, 1996]. In spite of all the drawbacks of the *Dst* index as a physical parameter [e.g., *Campbell*, 1996a,b], it is nonetheless a good measure of the overall strength of the near-Earth electric currents. As shown below, the inclusion of the *Dst* index improves the correlation between the predicted and observed lobe magnetic field. It should be noted that using the standard *Dst* index as a parameter in specification models is hindered by the fact that it cannot be provided in real time, since it requires a baseline derived from the quietest day data. However, there exist proxy techniques to obtain a near-real time *Dst* from ground geomagnetic data. Also, the *Dst* index can be predicted with a sufficient accuracy, using only the solar wind data [*Burton et al.*, 1975; *Valdivia et al.*, 1997]. In the present study, a new higher-resolution index SYM-H [*Iyemori*, 1990] was used, along with the standard 1-hour *Dst* index.

2. Data

The tail magnetic field data for this study came from the magnetometer experiments onboard three spacecraft: ISEE 2, AMPTE/IRM, and Geotail. In order to identify the data taken in the tail lobes and separate them from the observations in the plasma sheet, the concurrent data of the plasma instruments were used, as described below in more detail.

The final tail lobe data set was divided into six subsets, corresponding to six consecutive intervals of the distance $\rho = (X_{\rm GSM}^2 + Y_{\rm GSM}^2)^{1/2}$ from the $Z_{\rm GSM}$ axis, as follows: $10-15$, $15-20$, $20-25$, $25-30$, $30-40$, and $40-60\,R_E$. These intervals corresponded to the first six intervals of the tailward distance in our earlier study of the shape of the tail current [*Tsyganenko et al.*, 1998], which made it easier to use its results in this work.

2.1. ISEE 2 data

ISEE 2 spacecraft was launched in October 1978 in a highly eccentric orbit with an inclination 28.77° and an apogee of 23 R_E, passing through the nightside magnetosphere during the spring months. More details on the orbit were given by *Ogilvie et al.* [1977], while the magnetic field and plasma experiments were described in detail by *Russell* [1978] and *Bame et al.* [1978], respectively.

In this work, we used 1-min average magnetic field data taken during the period from January 2, 1978, to April 8, 1980. The procedure of data selection included the following steps. First, data taken well outside the magnetosphere as well as those taken too close to Earth (closer than 4 R_E) were eliminated. Then a visual inspection of the data was made to filter out bad and questionable data that might include magnetosheath contamination and to allow a finer selection of the data taken within the magnetosphere. In fact, that part of the data processing was made in the early 1990s and produced a magnetospheric spacecraft database and a catalog of the ISEE intervals inside the magnetosphere. That effort was described in detail elsewhere [*Fairfield et al.*, 1994].

In order to select the tail lobe data of ISEE 2, a subset of 1-min averages of nightside **B** was created, using the catalog of *Fairfield et al.* [1994]. Then the intervals inside the plasma sheet were removed, identified by the requirement that the concurrent proton pressure did not exceed a critical threshold value $P_{\rm crit}$. This was specified as follows. Assuming a lobe field $B \sim 25$ nT at $X = -20\,R_E$, the corresponding magnetic pressure of 0.25 nPa was expected to equal the plasma pressure at the center of the plasma sheet at that tailward distance. Using this estimate, we chose $P_{\rm crit} = 0.01$ nPa, i.e., 4% of the plasma sheet pressure. Since the lobe field and the plasma sheet pressure decrease tailward and increase earthward, an appropriate correction factor was introduced, so that the final formula for the threshold pressure became

$$P_{\rm crit} = 0.01\,(R/20)^{2\alpha}\ . \qquad (3)$$

The value of α in the power index in (3) can be specified using the results of earlier studies of the tail lobe field gradient (see *Fairfield and Jones* [1996] for an overview). In the present work, a value $\alpha = -0.64$ was assumed, obtained from the radial variation of the lobe field as shown by *Yamamoto et al.* [1994] in their Figure 3, based on Geotail data. The above value is within the ballpark range of those found earlier by different authors; in any case, owing to a rather strict upper limit (0.01 nPa) on the pressure at $R = 20\ R_E$, it is unlikely that the results of this study would be significantly affected by a slightly different choice of α.

The last step in the data preparation was averaging the 1-min values of the lobe B over 5-min intervals and tagging them with the corresponding 5-min data on the solar wind state and the Dst index . The solar wind data for the ISEE 2 subset of the tail lobe data were provided by IMP 8 spacecraft. The basic procedures of the solar wind data preparation were described by *Tsyganenko et al.* [1999], and readers are referred to that paper for more details.

Since we were interested in the effects of the solar wind and IMF "prehistory" on the tail field, every 5-min average tail lobe **B** vector in the database was provided with a "trail" of 12 consecutive 5-min average values of the solar wind parameters (density N, speed V, and the IMF components) to ensure a continuous coverage by the solar wind data of the entire hour, immediately preceding each lobe field measurement. All tail field observations with incomplete solar wind and IMF data trails were excluded from the analysis.

Besides the interplanetary medium data, the records in the ISEE 2 subset were tagged with hourly average values of the Dst index. As described below, the AMPTE/IRM and Geotail subsets had available a higher resolution Dst field (SYM-H); unfortunately, that index did not exist for the period 1978-1980 covered by ISEE 2. Nevertheless, since, by contrast to the IMF data, the large-amplitude variations of the Dst field occur on a relatively large timescale, it is unlikely that using hourly averages instead of the higher-resolution data would significantly affect the results.

The final restriction was related to the fact that ISEE 2 had its apogee at significantly higher solar ecliptic latitudes than two other spacecraft used in this study, which resulted in a significantly wider coverage of the tail lobes in the Z_{GSM} direction. That would not matter in the middle and distant tail, where the lobe field is nearly uniform across the tail; however, at the ISEE 2 location ($R \sim 10-20\ R_E$) the large transverse gradients of B could introduce a significant scatter. In order to avoid that an additional requirement $|Z_{ISEE} - Z_N| \leq 5\ R_E$ was imposed upon the distance along the Z direction between the spacecraft and the expected position of the center of the current sheet Z_N, so that the observed B would better reflect the local magnitude of the cross-tail current. The distance Z_N was calculated using the formula of *Tsyganenko et al.* [1998] (see their (2)):

$$Z_N(Y) = R_H - G\frac{Y^4}{Y^4 + L^4}\sin\Psi\ , \qquad (4)$$

where the parameters R_H, G, and L define the dependence of the current sheet shape on the dipole tilt angle Ψ; their numerical values were adopted from the above referenced paper. Note that in the present study we ignored the IMF-induced effect of cross-tail current sheet twisting since it is quite small at ISEE 2 distances.

Following all the above restrictions, from the original 16,996 5-min data records, only 226 were found to satisfy all the requirements and were included in the final ISEE 2 data subset. The most dramatic reduction was due to the requirement of the continuous coverage by the solar wind data over the preceding 1-hour interval and the restriction upon the distance from the center of the current sheet.

2.2. AMPTE/IRM data

The AMPTE/IRM spacecraft was launched on August 16, 1984, into an elliptical orbit with an inclination of 28.6° and an apogee of 18.83 R_E. Like ISEE 2, it passed through the nightside magnetosphere during the spring months, but in contrast to ISEE 2, the apogees of AMPTE/IRM were located at much lower solar ecliptic latitudes (and to the south of the ecliptic plane). More details on the orbit were given by *Bryant et al.* [1985]; the same publication contains a description of the magnetometer [*Luhr et al.*, 1985] and of the plasma experiment [*Paschmann et al.*, 1985].

The original 4-s average magnetometer and plasma instrument data underwent an initial selection and averaging over 1-min intervals. At that stage, the data taken at $X_{GSM} < 0$ and inside an average model magnetopause were selected for further processing. The data came from two 6-month intervals, January 2 to June 30, 1985, and February 20 to July 8, 1986.

The next step was to select the lobe data with $P < P_{crit}$ using the same formula (3) for the threshold pressure. As in the case of ISEE 2 data, all the magnetic field data without concurrent plasma pressure information were omitted. In total, 15,047 1-min tail lobe field data records were obtained at this step.

The final procedure was to average the data over 5-min intervals and tag each record with the SYM-H index of *Iyemori* [1990] and with the solar wind data "trail" in exactly the same way as described above for the ISEE 2 data. The total number of data records in the final AMPTE/IRM subset was 512 (135 for 1985 and 377 for 1986).

2.3. Geotail data

The Geotail spacecraft was launched on July 24, 1992. Its orbit was specially designed to explore the deep magnetotail (down to $\sim 220\ R_E$) and to skim the magnetopause at a wide range of distances during its first 2 years of operation. In 1994 and 1995 the apogee was lowered down to $\sim 50\ R_E$ and then to $\sim 30\ R_E$, which provided excellent coverage of the middle and near magnetotail. Owing to the relatively low latitude of the Geotail's orbit in the solar ecliptical coordinate system, most of the tail data were taken within a short distance from the center of the plasma sheet. Nonetheless, owing to the flapping motion of the plasma sheet and because of its systematic seasonal/diurnal warping and its IMF-induced twisting, a significant portion of the data came from the tail lobes. The Geotail orbit and experiments were described elsewhere [*Nishida*, 1994; *Kokubun et al.*, 1994; *Mukai et al.*, 1994]; also, more details on the coverage by Geotail of the equatorial nightside magnetosphere were given in our earlier paper [*Tsyganenko et al.*, 1998].

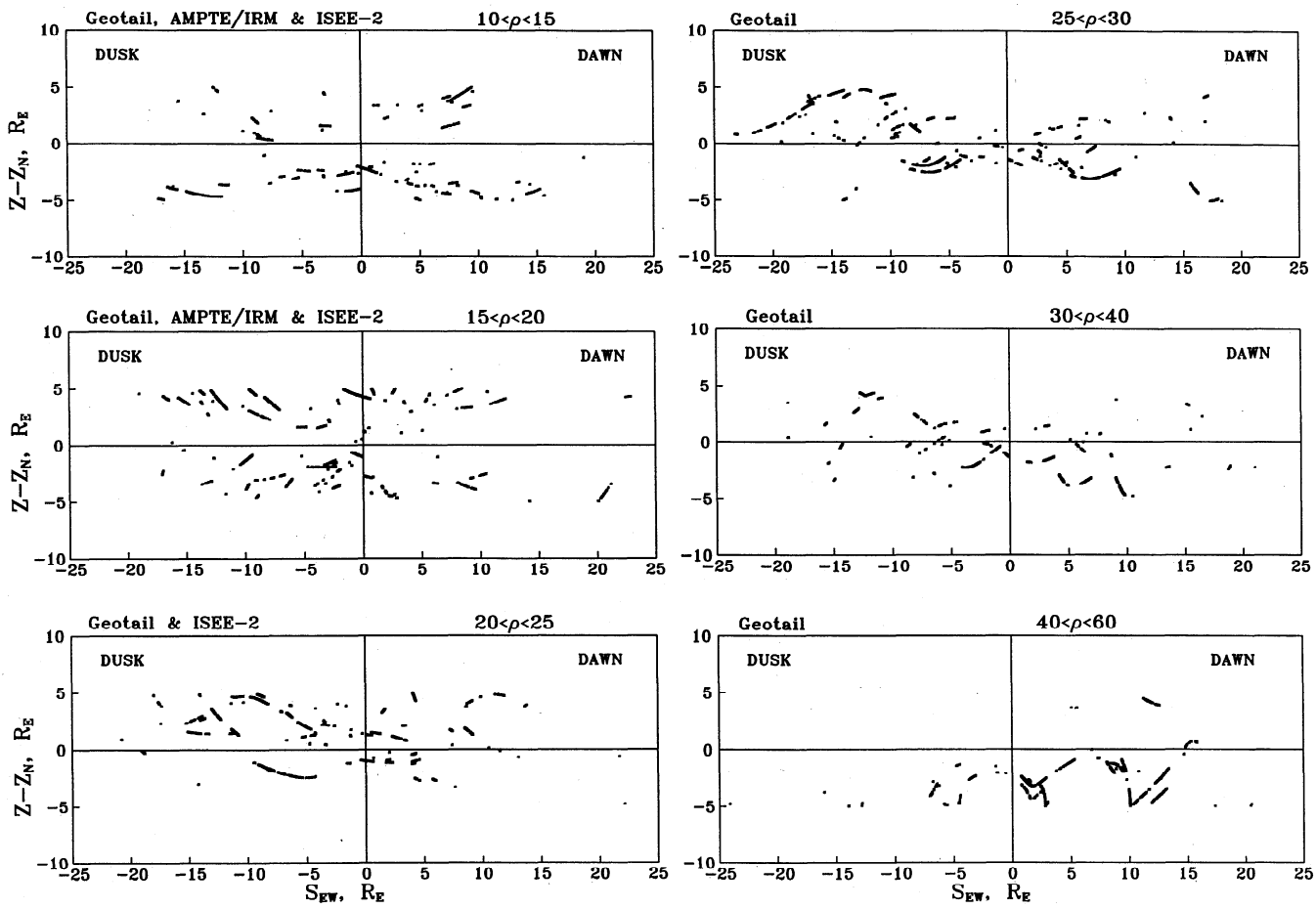

Figure 1. Spatial distribution of the lobe field data for six intervals of the distance ρ from the Z_{GSM} axis. The distance S_{EW} across the tail is measured along the cylindrical surfaces ρ = constant (horizontal axis), and the distance in the Z_{GSM} direction is measured from the position of the center of the cross-tail current, calculated for each data point using a corresponding value of the geodipole tilt angle.

In this work, the lobe measurements of Geotail were selected and processed using essentially the same procedure as described above for the ISEE 2 and AMPTE/IRM data. The magnetic field and plasma data covered the period from September 18, 1993, to December 22, 1997.

As in the case of AMPTE/IRM, the *Dst* field data for the Geotail subset were 5-min averages of the SYM-H index. Most solar wind data were taken by Wind spacecraft; a smaller portion was provided by IMP 8. Since most of the Wind observations were made relatively far from Earth, an appropriate time lag was introduced, based on the observed solar wind speed and the projection of the Earth–Wind distance on the Sun-Earth line. Special precautions were also made to exclude the data taken on solar wind flow lines passing too far from Earth. More details on the preparation of the solar wind data can be found elsewhere [*Tsyganenko et al.*, 1999].

After selecting the lobe data, averaging them over 5-min intervals, and tagging them with the solar wind data trails, the total number of the Geotail data records in the final subset was 2911. More details on the data distribution over individual bins of the tailward distance will be given in section 2.4.

2.4. Spatial distribution of the data

Figure 1 displays the spatial coverage by the data in the six bins of the distance ρ from the Z_{GSM} axis. Owing to the adopted way of the radial binning, the horizontal axis corresponds to the distance from the midnight meridian in the east-west direction $S_{EW} = \rho\phi$, measured along the cylindrical surface $\rho = \langle\rho\rangle$. The value of Z (vertical axis) assigned to each point is measured from the expected location Z_N of the center of the tail current sheet, estimated from (4) using the values of parameters R_H, G, and L, as found by *Tsyganenko et al.* [1998].

The first two bins of ρ contain data of all three spacecraft. Owing to the orbit limitations of AMPTE/IRM, the third bin ($20-25\,R_E$) is represented only by the data of ISEE 2 and Geotail, and as one proceeds farther tailward, Geotail remains the only source of data. However, because of the long time span of the data set the longitudinal coverage remains fairly uniform, except in the most remote bin ($40-60\,R_E$), where significantly more data came from the dawn side.

3. Tail lobe field: a linear regression model

In order to quantitatively represent the tail lobe field as a function of the solar wind state and the *Dst* field a linear regression relation was used,

$$B_{\text{lobe}} = B_0 + B_1\,(\rho - \langle\rho\rangle) + B_2\left(S_p - \langle S_p\rangle\right) + B_3\,(Dst - \langle Dst\rangle) + B_4\,(S_{\text{IMF}} - \langle S_{\text{IMF}}\rangle)\ , \qquad (5)$$

resembling the one used by *Nakai et al.* [1991] but differing from it in several respects. First, to take into account the radial variation of the magnetic field within each bin of ρ, a linear correction term with the coefficient B_1 was included in (5) from the outset, while Nakai et al. first normalized all their B values to the same location and then used them for the regression analysis. Second, as noted above, Nakai et al. assumed a linear dependence of B_{lobe} on the solar wind ram pressure P_d, while in this study, a more complex function S_p was used, specified below in more detail. Third, a linear dependence on the Dst field was added; as noted above, in the case of the ISEE 2 data it was a standard hourly Dst index, while for AMPTE/IRM and Geotail we used 5-min average values of the higher-resolution SYM-H index. Fourth, instead of the VB_z term, used by *Nakai et al.* [1991], several different IMF-related regressors S_{IMF} were explored in order to find the best one, as described below. Finally, no attempt was made here to include in the regression relation the solar wind thermal pressure and the AL index.

With regard to the spatial variation of the lobe field, the initial version of the regression relation (5) also included terms with a dependence on the azimuthal angle ϕ and on the distance $Z - Z_N$ from the expected position of the center of the current sheet, given by (4), and on the dipole tilt angle. However, those terms were found to provide a relatively small contribution to the lobe field magnitude and did not significantly improve the fit. For that reason, it was decided to retain, in the final expansion, only the radial term. In any case, an accurate description of the field's spatial structure should be pursued by means of full-scale three-dimensional modeling, while this work concentrates on the effects of the external factors on the tail current.

The pressure-dependent function S_p in (5) was represented as

$$S_p = \sum_{i=1}^{12} W_i f_i \Big/ \sum_{i=1}^{12} W_i \,, \tag{6}$$

where the summation covers twelve 5-min intervals, that is, 1-hour period immediately preceding any given tail field observation at the time t. The summation index i is related to the time lag $\tau_i = 5(i-1)$ (in minutes), so that the 5-min interval with $i = 1$ is the one of the actual lobe field observation, the one with $i = 2$ lags it by 5 min, etc. The response function $f_i = f(P_{di})$ gives the relative contribution to S_p by the solar wind pressure during the ith lag period; its concrete form is discussed in section 3.1. The weights W_i were introduced in order to vary the relative contributions from the solar wind states observed during 12 consecutive 5-min intervals. Thus, taking $W_1 = 1$ and $W_2 = W_3 = \ldots = W_{12} = 0$ would imply the "directly driven" mode of interaction, in which case only the current value of the solar wind pressure contributes to the control variable S_p. In contrast, assigning equal values to all 12 weights W_i would be equivalent to using uniform hourly averages. In this study, a simple continuous parameterization of the weight function by a single variable a_p was adopted, so that $W_i = W_i(\tau_i, a_p)$ (see appendix for more details). Assigning to a_p values from the interval $-2 < a_p < +2$ makes it possible to reproduce several qualitatively different basic modes of response; for example, taking $a_p = -1.9$ provides the directly driven mode; $a_p = -1$ yields a linearly decreasing sequence of W_i values; $a_p = 0$ results in a uniform weighting; $a_p = 1$ corresponds to a linear increase of W_i from 0 to 1 with growing time lag; and $a_p = 1.9$ yields a delayed pulse-like weight function, similar to the directly driven case, but lagged by 1 hour.

The IMF-related function S_{IMF} was represented in the same way as the pressure term, using the summation over 12 time intervals but with a set of weights, controlled by its own independent parameter a_{IMF}, so that

$$S_{\text{IMF}} = \sum_{i=1}^{12} W_i g_i \Big/ \sum_{i=1}^{12} W_i \,, \tag{7}$$

and $W_i = W_i(\tau_i, a_{\text{IMF}})$. Several forms of the function g were explored, containing different combinations of the interplanetary parameters. The results are described in section 3.1.

3.1. Choosing the solar-wind controlled response functions

The general procedure of choosing the regression functions began with a search for the best form of the pressure-related function f, entering in (6). At that step a plausible a priori form of the IMF-related term g was assumed. After the function f (and hence S_p) was specified, a detailed analysis of other possible candidates for g and S_{IMF} was made. At an initial phase of this study, a power law $f = P_d^{\alpha}$ was assumed for the response function f, where the best fit value of α was expected to be close to 0.5, as suggested by simple pressure balance considerations for the middle and distant tail. However, using smaller values of α gave a noticeable improvement of the correlation coefficient R (also called the multiple correlation coefficient) between the observed values of B and those predicted by (5).

That tendency was especially pronounced for two closest bins of the tailward distance $10 < \rho < 15$ and $15 < \rho < 20$: in these cases, choosing smaller and smaller values of α resulted in progressively higher correlation coefficients. In fact, the best fit values of α tended to zero, accompanied by unlimited growth of the regression coefficient B_2, which prompted us to assume $f = \ln P_d$, as an asymptotic limit of the power law with $\alpha \to 0$. That choice provided the best correlation between the observed and predicted field for $\rho \leq 20\, R_E$. At larger distances, using a power dependence instead of a logarithmic one yielded slightly higher correlations; for example, at $20 < \rho < 25$, the power dependence with $\alpha = 0.35$ gave the best result with $R = 0.8736$ (while the logarithmic function yielded $R = 0.8708$). In the most remote bin $40 < \rho < 60$, the best value of the power index was found to be $\alpha = 0.63$, with $R = 0.9182$, whereas for the logarithmic dependence we obtained $R = 0.9021$. However, in order to consistently describe the radial variation of the lobe field in the entire range of the distance and to compare the magnitudes of individual regression terms, we retained the logarithmic form of f for all the six bins of ρ.

With f and S_p thus defined, a search was made for the function g, entering the IMF-related term S_{IMF} in (7). Various functions, tried in this study, are listed in Table 1 along with the values of the multiple correlation coefficient R and of the rms deviation $\sigma = \langle \delta B_{\text{lobe}}^2 \rangle^{1/2}$. The functions are ordered by increasing values of R. Note that (1) all the results in Table 1 correspond to the closest interval of the distance $10 < \rho <$

Table 1. Values of the Correlation Coefficient R and of the rms Deviation σ, for 16 Different Combinations of the IMF-Related Parameters of the Solar Wind.

Combination	g	R	σ
1	B_z	0.9381	3.95
2	$B_\perp$	0.9426	3.80
3	B_s	0.9450	3.73
4	$B_\perp \sin(\theta/2)$	0.9468	3.66
5	$B_\perp \sin^2(\theta/2)$	0.9487	3.60
6	$B_\perp \sin^3(\theta/2)$	0.9492	3.58
7	$B_\perp^2$	0.9534	3.43
8	$B_\perp^2 \sin(\theta/2)$	0.9580	3.27
9	B_s^2	0.9602	3.18
10	$B_\perp^2 \sin^2(\theta/2)$	0.9608	3.16
11	$B_\perp^2 \sin^3(\theta/2)$	0.9626	3.09
12	$B_\perp^2 \sin^5(\theta/2)$	0.9639	3.03
13	$VB_\perp^2 \sin^2(\theta/2)$	0.9649	2.99
14	$VB_\perp^2 \sin^4(\theta/2)$	0.9650	2.99
15	$VB_\perp^2 \sin^3(\theta/2)$	0.9652	2.98
16	$Vh(B_\perp) \sin^3(\theta/2)$	0.9659	2.95

The results correspond to the nearest bin $10 < \rho \leq 15\ R_E$. The rms deviation $\sigma = \langle \delta B_{\text{lobe}}^2 \rangle^{1/2}$.

15 R_E and (2) the weights W_i for both the pressure- and IMF-related functions were calculated using $a_p = a_{\text{IMF}} = 0$, that is, assuming uniform averaging of both quantities over the 1-hour interval.

In general, the correlation coefficients in all cases are quite large, ranging between 0.94 and 0.97. The simplest choice $g = B_z$ yielded the lowest correlation (0.9381), while for $g = B_\perp = (B_y^2 + B_z^2)^{1/2}$ it is significantly higher. Choosing $g = B_s \equiv \min\{0, B_z\}$ (i.e., taking into account only southward values of IMF B_z), resulted in a further improvement, more clearly visible in the values of the rms deviation σ.

Introducing powers of $\sin(\theta/2)$, where θ is the IMF clock angle, yields even higher correlations, in most cases exceeding 0.96. The best result (line 12) among that kind of function was provided by $g = B_\perp^2 \sin^5(\theta/2)$, which gave $R = 0.9639$ and $\sigma = 3.03$. Further improvement can be achieved by multiplying the IMF-related group of factors by the solar wind speed V (lines 13–16). Finally, one may expect that for sufficiently high magnitudes of the IMF the quadratic dependence of B_{lobe} on $B_\perp$ should gradually transform into the linear one (as it appears from a simple model with superposed terrestrial and interplanetary fields). This conjecture was tested by introducing the function

$$h(B_\perp) = \frac{(B_\perp/B_c)^2}{1 + B_\perp/B_c}, \tag{8}$$

where B_c is a characteristic value of $B_\perp$ corresponding to the transition from the quadratic to the linear law. In line 16 of Table 1 the results are given for $g = Vh(B_\perp)\sin^3(\theta/2)$ with $B_c = 40nT$, a value that provided the highest correlation coefficient $R = 0.9659$.

Before proceeding further, a comment should be made on the degree of mutual independence of the individual input variables and on the relative importance of the regression terms in (5). As expected, the radial distance ρ was found to be virtually uncorrelated with Dst, S_p, and S_{IMF}, with the correlation coefficients equal to –0.11, –0.02, and –0.04, respectively. The correlation between the pressure term S_p and Dst was also quite low ($R = -0.12$), but it was found significantly higher between S_p and S_{IMF} ($R = 0.44$) as well as it was between Dst and S_{IMF} ($R = -0.49$). To check the relative importance of various regression terms, the correlation coefficients were rederived for versions of (5) missing one term, i.e., lacking dependence on ρ ($B_1 = 0$), on the pressure ($B_2 = 0$), on Dst ($B_3 = 0$), or on the IMF ($B_4 = 0$). These gave a decrease of the correlation coefficient from 0.966 to 0.843, 0.899, 0.954, and 0.908, respectively. From this, one might conclude that the radial variation has the largest effect on the multiple correlation, the pressure- and IMF-related terms are of approximately equal importance and share the second place, while the Dst field has the weakest correlation with B_{lobe}. However, as noted earlier, S_p, Dst, and S_{IMF} are not quite independent of each other, and therefore the above ranking may be questioned. An alternative way of ranking regression terms is to calculate the partial correlation coefficients. That method suggested a somewhat different ordering of the input variables by their importance: The largest partial correlation coefficient (0.7399) was obtained for S_{IMF}, followed by S_p (0.6704), ρ (–0.5490), and Dst (–0.4438).

3.2. Effects of the weighted time-lagged response in the near tail

The next task was to explore the effect of changing the time-lagged weight profiles in the pressure- and IMF-related regression terms. Using the chosen response functions

$$f = \ln(P_d) \qquad g = Vh(B_\perp)\sin^3(\theta/2), \tag{9}$$

Table 2. Parameters of Data Subsets and Regression Coefficients for Consecutive Bins of ρ

		$10<\rho<15$	$15<\rho<20$	$20<\rho<25$	$25<\rho<30$	$30<\rho<40$	$40<\rho<60$
				Data Set			
N		359	624	527	776	412	640
$\langle B_{\rm lobe}^2\rangle^{1/2}$		43.61	29.18	21.99	20.70	18.71	14.53
$\langle\rho\rangle$		12.79	17.72	22.79	27.81	32.66	45.36
$\langle S_p\rangle$		0.7236	0.7389	0.6745	1.031	1.080	0.7883
$\langle Dst\rangle$		−20.67	−14.06	−15.97	−7.64	−6.38	−6.49
$\langle S_{\rm IMF}\rangle$		3.663	2.126	2.183	2.118	2.087	3.081
	Term in (5)			*Regression Parameters*			
B_0	1	42.10±0.15	28.57±0.10	21.26±0.12	20.45±0.08	18.37±0.10	13.74±0.08
B_1	$\rho-\langle\rho\rangle$	−4.19±0.12	−1.24±0.08	−1.02±0.09	−0.62±0.07	−0.574±0.038	−0.069±0.034
B_2	$S_p-\langle S_p\rangle$	10.55±0.40	8.17±0.29	8.48±0.35	5.27±0.29	5.99±0.48	5.54±0.21
B_3	$Dst-\langle Dst\rangle$	−0.177±0.015	−0.078±0.009	−0.022±0.008	−0.065±0.008	0.012±0.016	0.053±0.008
B_4	$S_{\rm IMF}-\langle S_{\rm IMF}\rangle$	0.866±0.035	0.749±0.043	0.626±0.060	0.372±0.043	0.484±0.082	0.386±0.030
σ		2.88	2.58	2.78	2.31	2.10	2.04
R		0.9675	0.9007	0.8675	0.7069	0.8065	0.9012
a_p		1.45	−0.80	−1.40	−1.40	−1.75	−0.20
$a_{\rm IMF}$		0.15	0.70	−1.30	−1.40	0.70	−1.10

a search was made in each bin of ρ for an optimal pair of values of a_p and $a_{\rm IMF}$, minimizing the rms deviation σ. In the nearest bin of the tailward distance, the optimal values $a_p = 1.45$ and $a_{\rm IMF} = 0.15$ were found to further increase the correlation coefficient from $R = 0.9659$ to $R = 0.9675$ and decrease the rms deviation σ from 2.95 to 2.88. While it appears as insignificant improvement, the effect of introducing the weighted response appears more convincing if we compare the last figures with those calculated under assumption of a nearly instantaneous (directly driven) mode of the solar wind control by taking $a_p = -1.9$ and $a_{\rm IMF} = -1.9$. Using the latter values yielded a clearly worse fit with $R = 0.9447$ and $\sigma = 3.73$.

The assumed simple form of the weight function $W(\tau, a)$ did not comprise all possible options (e.g., choosing a weight function with a peak in the middle of the 1-hour trail interval, or taking longer averaging intervals). Also, no attempt was made to quantitatively assess the statistical uncertainties of the obtained a_p and $a_{\rm IMF}$. With these reservations in mind, note that the value $a_p = 1.45$, obtained for the nearest bin of distance, implies a considerable delay of the near tail response to the solar wind pressure variations. A probable explanation is that, besides the direct compression/expansion of the magnetopause (which results in an almost immediate response of $B_{\rm lobe}$), a significant contribution comes from the relatively slow earthward shift of the cross-tail current during disturbed periods with large P_d. The tailward variation of the weighted response parameters a_p and $a_{\rm IMF}$ will be discussed in the next section, and a more general treatment of the problem is described in section 3.4.

3.3. Tailward variation of the lobe field parameters

The values of the regression coefficients with their error estimates, as well as the characteristics of the data subsets for all six intervals of ρ are given in Table 2. The first six rows contain the quantities characterizing the data subsets, such as the number of the data points, rms values of $B_{\rm lobe}$, and the average values of the parameters entering in the regression relation (5). The bottom of Table 2 presents the obtained best fit values of the regression coefficients, the rms deviation σ, and the multiple correlation coefficient R. The last two lines contain the estimates of the parameters of the weight functions for the pressure- and IMF-related terms. The estimates of the uncertainties are made on the premise that the chaotic component in the lobe field is distributed according to Gaussian law [e.g., *Bevington,* 1969], which is not an obvious assumption. It is also important that in calculating the uncertainties we tacitly assumed that the values of the solar wind parameters did not contain errors and corresponded to their actual values near the Earth's orbit. Since a significant fraction of those data came from Wind spacecraft, located far upstream, one should be aware that the actual errors can be significantly larger. Section 4 contains further discussion of the statistical uncertainties.

The coefficients B_0 and B_1 represent the average lobe field within a bin and its radial gradient; as expected, both of them monotonically decrease with growing tailward distance. The coefficient B_2 is a measure of the tail field variation in response to the changes in the solar wind dynamic pressure; it also decreases tailward, although in a less orderly manner and more slowly than the average lobe field. As a result, the field in the middle tail is relatively more sensitive to variations of P_d than it is in the near tail; thus, a fivefold increase of P_d from 2 to 10 nPa would result in a $\sim$ 40% increase of the field (from 42 to 59 nT) at $\rho \sim 12\,R_E$, while at $\rho \sim 40\,R_E$ the relative increase of $B_{\rm lobe}$ would amount to $\sim$ 60% of its original magnitude.

The coefficient B_3 relating the response of $B_{\rm lobe}$ to the Dst field is quite significant in the innermost bin. More specifically, the same increase in the lobe field from 42 to 59 nT, as in the above example for P_d, would require a drop in the

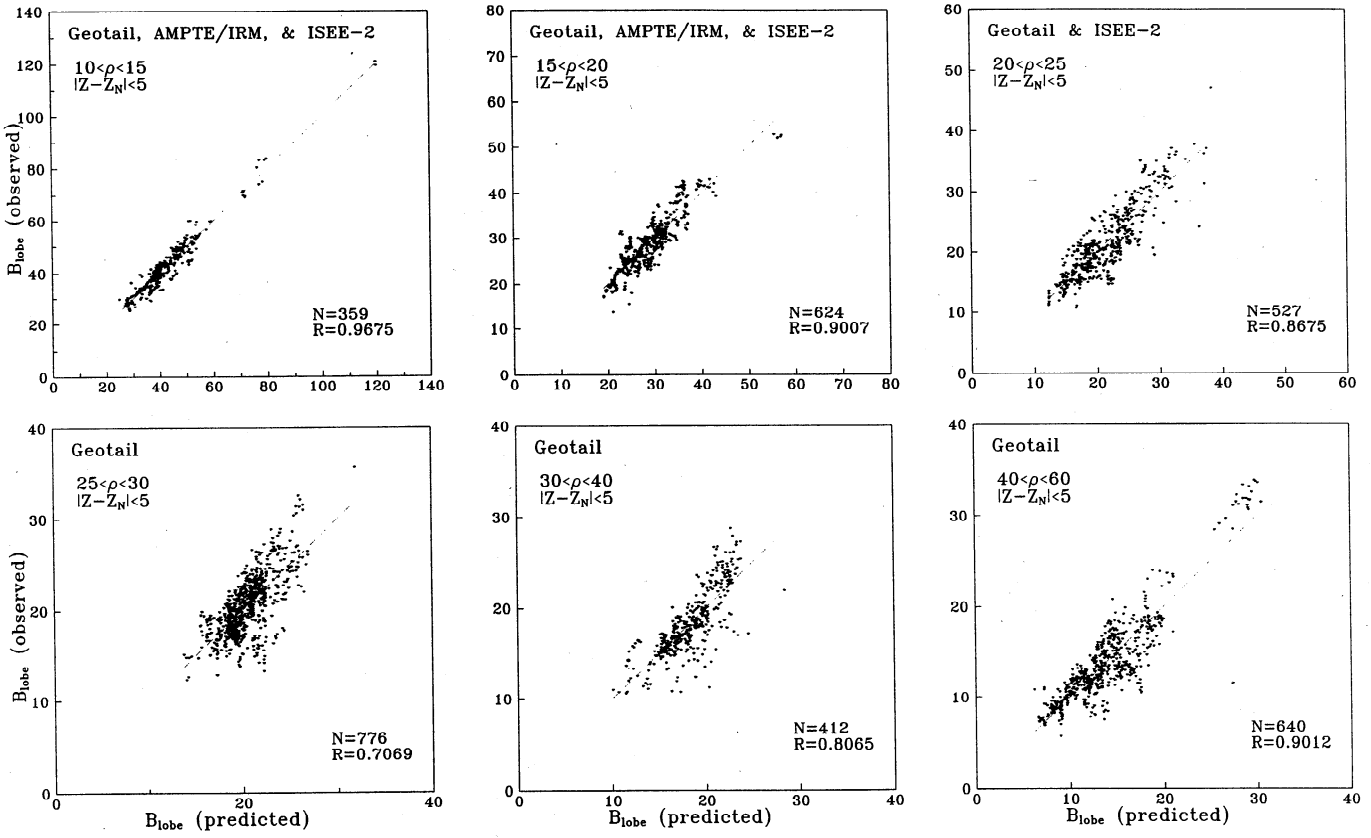

Figure 2. Scatterplots of the observed tail lobe field values against those predicted by the regression relationship (5) for six intervals of the distance ρ. Best linear fits are shown by dashed lines.

Dst index by about -100 nT (assuming that other variables do not change). However, B_3 rapidly falls off with growing distance and becomes negligibly small even at $\rho \geq 20\,R_E$, which implies that only the near-Earth part of the tail current makes a tangible contribution to the *Dst* field on the ground.

The IMF-related coefficient B_4 decreases with growing ρ, at approximately the same rate as the pressure-related coefficient B_1. The relative importance of the corresponding IMF-related term in (5) can be clarified by the following example: For IMF $B_y = 0$, $B_z = -10$ nT, and $V = 400$ km/s the contribution from the IMF-related term to the lobe field in the innermost bin 10–15 R_E equals $\sim$ 17 nT; that is, it has approximately the same effect as the fivefold increase of P_d. At larger distances the IMF-related term contributes less in terms of the absolute value but becomes more significant in the relative sense because of the faster tailward decrease of the average field.

The correlation coefficient R decreases with growing radial distance from $R \approx 0.97$ at $10 < \rho < 15$ to $R \approx 0.71$ at $25 < \rho < 30$ and then increases back to $R \approx 0.90$ at $40 < \rho < 60$. Regarding the tailward decrease of R, observed within first four bins, it can be attributed to the following factors. First, the tail field becomes progressively noisier and less ordered with growing distance from Earth, even in the lobes. Second, because of the rapid decrease of the field radial gradient the contribution from the second term in (5) becomes smaller at larger distances. In addition, the magnitude of the *Dst* related term dramatically falls off with growing ρ. In the modeling terms this can be viewed as a reduction of the number of degrees of freedom of the regression relation (5), which explains the decrease of R. It still remains not quite clear why the correlation coefficient raises again beyond $25 < \rho < 30$. A possible cause could be a significantly smaller number of the data points in the interval $30 < \rho < 40$ and the presence of an isolated group of data points with unusually large $B_{\text{lobe}} \sim 30$ nT in the most remote interval $40 < \rho < 60$ (those data came from an extremely disturbed period in the early UT hours of December 24, 1994). However, even after that group of points was excluded from the calculation, the correlation coefficient remained as high as 0.83, which is still larger than for the neighbor earthward bin. A possible interpretation of this finding will be given in section 4.

The above results are illustrated by a sequence of scatterplots of the predicted lobe field values (5) against the observed ones, which are displayed in Figure 2 for all six intervals of the distance. In the nearest bin, $10 < \rho < 15$, most of the data concentrate within the interval 20–60 nT; there is also a relatively sparse group of data points with larger $B \sim 80$ nT, provided by Geotail observations during three disturbed days in 1995 and in 1997, and, finally, two data points with extremely large $B \sim 120$ nT, which came from the ISEE 2 data set (day 52 of 1979). The other plots show similar patterns of the data distribution. As one proceeds from closer to more distant bins, the data clouds become more dispersed and shift to smaller values of B, reflecting the increase in the tail field variability with growing distance and its decreasing magnitude. In all cases, the clouds abruptly terminate at a significant distance from the origin, ranging from $\sim$ 25 nT

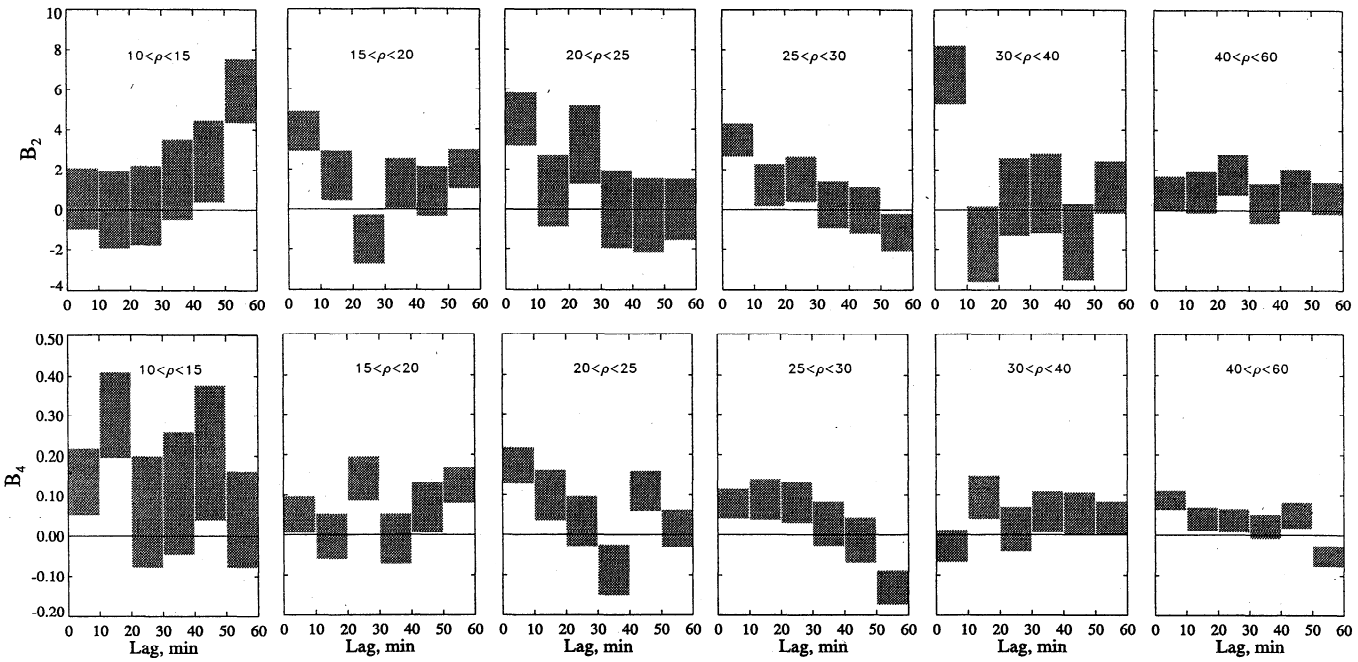

Figure 3. Distributions of the values of the weight coefficients B_2^k (pressure-related term) and B_4^k (IMF-related term) over the 1-hour interval of the lag time for six intervals of the tailward distance ρ. The width of the shaded bars corresponds to 10-min intervals of the lag time, and their height indicates the statistical uncertainty.

for $10 < \rho < 15$ to $\sim$ 8 nT for $40 < \rho < 60$. This is an indirect evidence that the selection of the lobe intervals using the plasma data and the threshold pressure (3) effectively eliminated all observations in the plasma sheet.

The time-weighting parameters a_p and a_{IMF} also reveal an interesting variation with ρ, although not as orderly as in the case of the regression coefficients. As one proceeds to larger distances, the parameter a_p rapidly decreases from 1.45 at $10 < \rho < 15$ down to -1.75 for $30 < \rho < 40$, indicating a change in the response mode, from the significantly delayed one to nearly directly driven. In the farthest bin, $40 < \rho < 60$, the parameter a_p sways back to a relatively small value -0.20, which may result from the increasingly large propagation time of the lobe compression tailward from Earth (note that all the times in our solar wind database were recalculated based on Wind and IMP 8 location relative to Earth rather than to the spacecraft in the tail). The behavior of the parameter a_{IMF} is more erratic than of a_p, but one still can discern the same tendency: positive values in the nearest bins, large negative values farther out in the middle tail, and some fluctuation in the farthest bins.

3.4. Time-lagged response: an alternative method

As noted earlier, the adopted simple one-parameter form of the weighting function for the pressure- and IMF-related terms does not exhaust all possible choices; in addition, the above results did not give any clue on the uncertainties involved, which left us with a sense of incompleteness. In order to better resolve the time lag effects, a further study was made using a different method.

Namely, instead of weighting the 5-min values of the response functions f and g by a predetermined set of normalized weights W_i, as specified by (6) and (7), the weights themselves were treated as unknown coefficients. More specifically, the regression form (5) was modified, so that the terms $B_2(S_p - \langle S_p \rangle)$ and $B_4(S_{\mathrm{IMF}} - \langle S_{\mathrm{IMF}} \rangle)$ were replaced by the sums

$$\sum_{k=1}^{6} B_2^{(k)}(f_k - \langle f_k \rangle) \qquad \sum_{k=1}^{6} B_4^{(k)}(g_k - \langle g_k \rangle)\,. \tag{10}$$

Note that, in contrast to (6) and (7), here we have only six terms in each sum, representing the response of the lobe field to six consecutive 10-min average values of f and g from the 60-min interval immediately preceding the B_{lobe} measurement. In principle, we could retain in the summation all twelve 5-min average values of f_k and g_k; however, that would further increase the number of unknown parameters and, hence, rise their uncertainties beyond the acceptable level. On the basis of the results given below, we believe that the adopted division of the hourly intervals into six 10-min intervals is close to an optimal choice.

Figure 3 displays the plots of the individual response amplitudes $B_2^{(k)}$ (top) and $B_4^{(k)}$ (bottom), corresponding to the functions f_k and g_k, respectively, as functions of the time lag, proportional to the index k. The height of the shaded bars shows the statistical uncertainty. The results, in general, agree with the previously discussed findings, based on the analysis of the parameters a_p and a_{IMF}. In the nearest bin of ρ the coefficient B_2 remains relatively small at small time lags but rapidly increases as the lag exceeds 30 min. At larger distances its behavior is quite different: In all the plots but the last one, the largest contribution comes from the most recent bin of the time lag, implying that the directly driven response to the solar wind pressure dominates in most of the tail.

The distribution of the coefficient B_4 is, in general, more chaotic. In the nearest bin of the distance, there is a distinct peak at the lag of 10-15 min, but overall, the shape of the profile is more evenly distributed over the entire span of the time lags. In the next bin, $15 < \rho < 20$, the peak of the IMF-related response function is shifted to 20-30 min, while at larger distances the largest contribution corresponds to small and intermediate time lags.

4. Discussion and conclusions

Before summarizing the results, a comment should be made on an important aspect of our regression analysis. Specifically, in spite of the apparently large number of individual 5-min averages in the radial distance bins, one should be aware that most of the tail lobe data are grouped in clusters, each containing several (from 3 to $\sim$ 30–50) consecutive data points, taken on single passes of the spacecraft. In many cases both the tail lobe field and the controlling parameters of the solar wind vary on a timescale significantly > 5 min. Therefore the consecutive data points within each cluster are not quite independent of each other, which can result in deceptively low values of the statistical uncertainties of the regression coefficients. Since the uncertainties are inversely proportional to the square root of the number of independent measurements, the actual values of the uncertainties can be significantly larger than those given in Table 2. A rough evaluation of the effect can be made, taking into account that the number of the data clusters from different passes was between 10 and 20% of the total number of individual data points in our subsets. On the basis of this estimate, we conclude that the actual uncertainties can exceed those in Table 2 by a factor of 2-3.

In summary, a study was made here of the tail lobe field response to the state of the incoming solar wind, using the magnetometer and plasma instrument data of three spacecraft, taken in a wide range of tailward distances and local times during three separate periods between 1978 and 1997. Owing to the large size of the initial database a relatively large set of lobe measurements was compiled, and each tail field record was provided with a continuous sequence of 12 values of 5-min average solar wind and IMF parameters during the preceding hour. A linear regression relationship was derived between the tail lobe field strength, a solar-wind pressure parameter S_p, the Dst field on the ground, and an IMF-related parameter $S_{\rm IMF}$ for six bins of radial distance between 10 and 60 R_E.

A detailed search was made for the best combination of the solar wind pressure- and IMF-related parameters, providing the highest value of the multiple correlation coefficient R and the lowest rms deviation σ between the predicted and observed lobe field. A simple four-parameter regression relation was found to yield a very good fit ($R = 0.967$ and $\sigma/\langle B^2\rangle^{1/2} = 0.066$) in the nearest bin of the distance $10 < \rho < 15$. It was found that the near-tail lobe field becomes significantly less sensitive to the solar wind pressure for large values of P_d, so that it can be best described by a logarithmic dependence, while a power law $f = P_d^{\alpha}$ with any value of the index α yielded persistently worse results. Our initial guess was that the weaker response of the near-tail lobe field to P_d was due to a relatively large contribution from the Earth's dipole to the total B in that region. To check this conjecture, we fitted the external part of the total field (i.e., with the dipole part removed), using the same regression relation (5). Surprisingly, the external field showed the same behavior as the total one, that is, a clear preference for the slower logarithmic response to P_d in the near tail. This finding is in line with the result of *Fairfield and Jones* [1996], who demonstrated a significantly slower dependence of the tail lobe field on the external dynamic pressure (fourth root) than the linear response assumed by *Nakai et al.* [1991].

Among various IMF-related functions the best results for the near tail were obtained with $g = Vh(B_\perp)\sin^3(\theta/2)$, where the function h, given by (8), behaves as $B_\perp^2$ for weak IMF but gradually transforms into a linear dependence for $B_\perp \geq 40nT$. It should be noted that for small $B_\perp$ the above function g is quite close to the ϵ index of *Akasofu* [1979].

A comparison of the partial correlation coefficients showed that the IMF- and pressure-related terms are the most important ones since they (1) provide the largest contribution to the predicted lobe field at all tailward distances and (2) have the largest partial correlation coefficients with $B_{\rm lobe}$.

The Dst term yields a significant contribution to the regression relation in the nearest bin of ρ, suggesting that the fringe field of the near-tail current sheet contributes to Dst at Earth's surface, especially during disturbed times. However, judging from the obtained values of the corresponding correlation coefficients, the relative importance of the Dst as a predicting variable is smaller. In addition, the Dst-related coefficient rapidly falls off to zero at larger distances.

Using the same regression relationship (5) for representing the tail lobe field at larger distances yielded the radial variation of the tail lobe field and its response to the external parameters. While the absolute magnitude of the mean field B_0 and of all the regression terms decreased with growing distance, the relative amplitude of the externally induced variations against the average $\langle B_{\rm lobe}\rangle$ was found to increase tailward. As expected, the correlation coefficient R was found to decrease with growing ρ within first four bins of the distance. However, in the two farthest bins that trend was reversed, probably because of the fact that the middle tail ($\rho \sim 25\ R_E$) appears as a transition region between two different regimes and, as such, is most affected by the substorm-related instabilities. At closer distances, the tail field becomes more ordered, due to the growing contribution of the Earth's field, while at larger distances the tail configuration becomes fully established and thus relatively more stable.

A study of the time lag effects was also made by using the data from 1-hour trails of the solar wind parameters, accompanying each lobe field data record. Two methods were employed, in which the contributions from the solar wind pressure- and IMF-related terms were represented as weighted sums over 1-hour periods, immediately preceding the lobe field measurements. For the nearest interval of the distance, the best fit weight function for the pressure-dependent term was found to rapidly increase with growing time lag, suggesting a significant average delay between the changes of the solar wind pressure and the reaction of the lobe field. However, one has to keep in mind the statistical nature of the result; in individual cases the sequence of

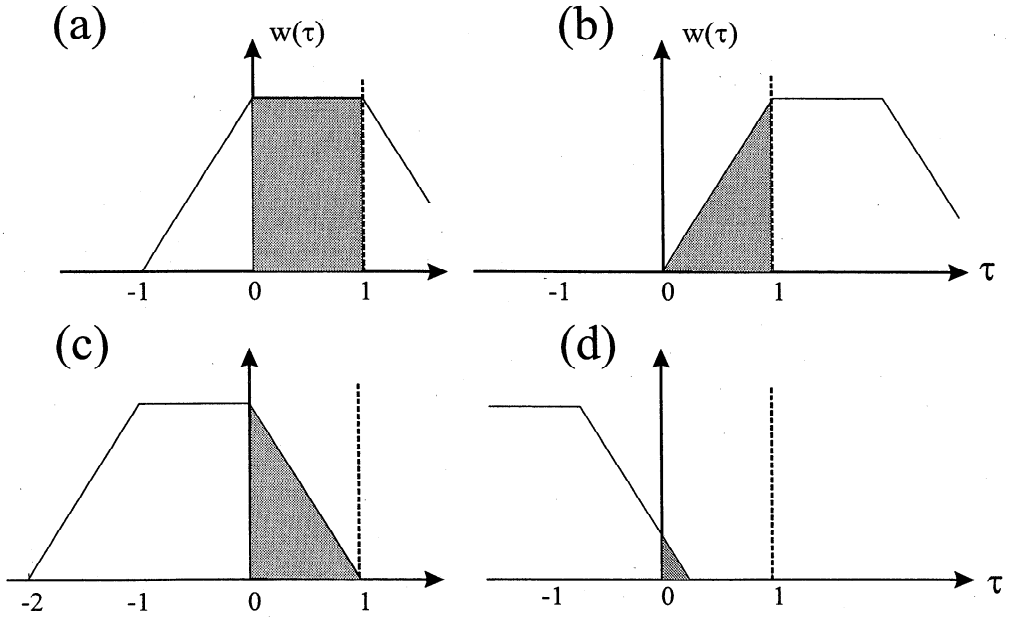

Figure A1. Example plots of the weight function $W(\tau, a)$ against the time lag τ for four values of the shift parameter a. (a) Here $a = 0$: uniform averaging over the 1-hour trail of the solar wind data, (b) $a = 1$: linearly increasing weight function (mostly delayed response), (c) $a = -1$: linearly decreasing weight function (mostly directly driven response), and (d) $a \approx -1.7$: almost instantaneous response. The shaded areas correspond to the lags τ with $W \neq 0$.

events can be more complex, combining an almost immediate change in the lobe field due to changing magnetopause current and a delayed growth/decrease of the field in response to the convective transport effects in the plasma sheet.

The weight functions, derived for more distant bins, in most cases maximize at or shortly after the time of the lobe field observation and then decrease with growing time lag. This implies that the directly driven mode of response prevails in the middle and distant tail.

The obtained results have several implications with regard to the parameterization of the cross-tail current in the magnetospheric models. (1) The square root dependence of the tail current, adopted in the T96 model, should be replaced by a slower one, which can be either the logarithmic function (9) (in the near-tail region) or a power law with $\alpha < 0.5$ (in the middle tail). (2) The IMF dependence can be best represented by the function g, given by (9). (3) Information on the prehistory of the external input is important and can be taken into account by integrating the solar wind control functions (with appropriate weight functions) over an hour-long interval, immediately preceding the moment of the tail field measurement (or modeling). (4) Inclusion of the *Dst* index in the amplitude factor of the near-tail current can distinctly improve the accuracy.

Appendix. Weight Function for the Time-Lagged Solar Wind Parameters

The values W_i of the weight function in (6) and (7) were defined as

$$W_i = W(\tau_i, a) = p(\tau_i - a)q(\tau_i)\,, \qquad \text{(A1)}$$

where $\tau_i = i/12$ $(1 \leq i \leq 12)$ is the time lag for the ith 5-min interval (in units of the fraction of an hour). The function $p(\tau)$ in (A1) has a trapezoidal profile given by

$$p(\tau) = \begin{cases} \tau + 1 & \text{if } -1 < \tau < 0 \\ 1 & \text{if } 0 < \tau < 1 \\ 2 - \tau & \text{if } 1 < \tau < 2 \\ 0 & \text{otherwise} \end{cases} \qquad \text{(A2)}$$

and the second factor in (A1) is the "gate" function

$$q(\tau) = \begin{cases} 1 & \text{if } 0 < \tau < 1 \\ 0 & \text{otherwise}\,. \end{cases} \qquad \text{(A3)}$$

Varying the parameter a within the interval $-2 < a < 2$ provides a shift of the factor p along the time axis, which results in several different types of the weight function distributions over the 1-hour trail of the solar wind data, shown in Figure A1 by shading. Note that, owing to the normalization in (6) and (7), the absolute values of the weights W_i (and hence the apparent inequality of the shaded areas) do not matter.

Acknowledgments. The author thanks the IMP 8 and Wind Magnetometer Data Processing Teams for the IMF data of those spacecraft, Keith Ogilvie for providing the solar wind plasma data of Wind, and Al Lazarus for providing the solar wind plasma data of IMP 8. The Geotail magnetic field and plasma data were kindly provided by Susumu Kokubun and Toshifumi Mukai. The ISEE 2 magnetometer and Fast Plasma Experiment (FPE) data were provided to the National Space Science Data Center (NSSDC) courtesy of Chris Russell, Goetz Paschmann, and Jack Gosling. The AMPTE/IRM magnetometer and plasma instrument data were made available by the Hermann Luhr and Goetz Paschmann. All of the above principal investigators are gratefully acknowledged. Thanks are due to Peter Karlsson for his assistance in analyzing

the ISEE 2 FPE data, to Toshihiko Iyemori for providing the SYM and ASYM geomagnetic indices, and to David Stern and Victor Sergeev for their constructive comments on the first draft of the manuscript. The interplanetary medium data were retrieved using the NSSDC on-line facilities (SPYCAT and CDAWEB). This work is supported by NASA grants NASW-97024 (ISTP GI Program), and NSF Magnetospheric Physics Program grant ATM-9819873.

Janet Luhmann thanks Steven Petrinec and another referee for their assistance in evaluating this paper.

References

Akasofu, S.-I., Interplanetary energy flux associated with magnetospheric substorms, *Planet. Space Sci., 27,* 425, 1979.

Bame, S. J., J. R. Asbridge, H. E. Felthauser, J. P. Glore, G. Paschmann, P. Hemmerich, K. Lehmann, and H. Rosenbauer, ISEE-1 and ISEE-2 fast plasma experiment and the ISEE-1 solar wind experiment, *IEEE Trans. Geosci. Electr., GE-16,* No. 3, 216, 1978.

Bevington, P. R., *Data Reduction and Error Analysis for the Physical Sciences,* McGraw-Hill, New York, 1969.

Bryant, D. A., S. M. Krimigis, and G. Haerendel, Outline of the Active Magnetosphere Particle Tracer Explorers (AMPTE) mission, *IEEE Trans. Geosci. Remote Sens., 23(3),* 177, 1985.

Burton, R. K., R. L. McPherron, and C. T. Russell, An empirical relationship between interplanetary conditions and *Dst, J. Geophys. Res., 80,* 4204, 1975.

Campbell, W. H., Geomagnetic storms, the Dst ring-current myth and lognormal distribution, *J. Atmos. Terr. Phys., 58,* 1171, 1996a.

Campbell, W. H., Dst is not a pure ring-current index, *Eos Trans. AGU, 77(30),* 283, 1996b.

Fairfield, D. H., and J. Jones, Variability of the tail lobe field strength, *J. Geophys. Res., 101,* 7785, 1996.

Fairfield, D. H., N. A. Tsyganenko, A. V. Usmanov, and M. V. Malkov, A large magnetosphere magnetic field database, *J. Geophys. Res., 99,* 11,319, 1994.

Hilmer, R. V., and G.-H. Voigt, A magnetospheric magnetic field model with flexible current systems driven by independent physical parameters, *J. Geophys. Res., 100,* 5613, 1995.

Iijima, T., and T. A. Potemra, The relationship between interplanetary quantities and Birkeland current densities, *Geophys. Res. Lett., 9,* 442, 1982.

Iyemori, T., Storm-time magnetospheric currents inferred from mid-latitude geomagnetic field variations, *J. Geomagn. Geoelectr., 42,* 1249, 1990.

Kokubun, S., T. Yamamoto, M. H. Acuna, K. Hayashi, K. Shiokawa, and H. Kawano, The Geotail magnetic field experiment, *J. Geomagn. Geoelectr., 46,* 7, 1994.

Luhr, H., N. Klocker, W. Oelschlagel, B. Hausler, and M. H. Acuna, The IRM fluxgate magnetometer, *IEEE Trans. Geosci. Remote Sens., 23(3),* 259, 1985.

Maltsev, Y. P., A. A. Arykov, E. G. Belova, B. B. Gvozdevsky, and V. V. Safargaleev, Magnetic flux redistribution in the storm time magnetosphere, *J. Geophys. Res., 101,* 7697, 1996.

Mead, G. D., and D. H. Fairfield, A quantitative magnetospheric model derived from spacecraft magnetometer data, *J. Geophys. Res., 80,* 523, 1975.

Mukai, T., S. Machida, Y. Saito, M. Hirahara, T. Terasawa, N. Kaya, T. Obara, M. Ejiri, and A. Nishida, *J. Geomagn. Geoelectr., 46,* 669, 1994.

Nakai, H., Y. Kamide, and C. T. Russell, Influences of solar wind parameters and geomagnetic activity on the tail lobe magnetic field: A statistical study, *J. Geophys. Res., 96,* 5511, 1991.

Nishida, A., The Geotail mission, *Geophys. Res. Lett., 21,* 2871, 1994.

Ogilvie, K. W., T. von Rosenvinge, and A. C. Durney, International Sun-Earth Explorer: A three-spacecraft program, *Science, 198(4313),* 131, 1977.

Ostapenko, A. A., and Yu. P. Maltsev, Relation of the magnetic field in the magnetosphere to the geomagnetic and solar wind activity, *J. Geophys. Res., 102,* 17,467, 1997.

Paschmann, G., H. Loidl, P. Obermayer, M. Ertl, R. Laborenz, N. Sckopke, W. Baumjohann, C. W. Carlson, and D. W. Curtis, The plasma instrument for the AMPTE IRM, *IEEE Trans. Geosci. Remote Sens., 23(3),* 262, 1985.

Russell, C. T., The ISEE 1 and 2 fluxgate magnetometers, *IEEE Trans. Geosci. Remote Sens., 16(3),* 239, 1978.

Tsyganenko, N. A., Global quantitative models of the geomagnetic field in the cislunar magnetosphere for different disturbance levels, *Planet. Space Sci., 35,* 1347, 1987.

Tsyganenko, N. A., A magnetospheric magnetic field model with a warped tail current sheet, *Planet. Space Sci., 37,* 5, 1989.

Tsyganenko, N. A., Modeling the Earth's magnetospheric magnetic field confined within a realistic magnetopause, *J. Geophys. Res., 100,* 5599, 1995.

Tsyganenko, N. A., Effects of the solar wind conditions on the global magnetospheric configuration as deduced from data-based field models, *Eur. Space Agency Spec. Publ., ESA SP-389,* 181, 1996.

Tsyganenko, N. A., Data-based models of the global geospace magnetic field: Challenges and prospects of the ISTP era, in *Geospace Mass and Energy Flow: Results From the International Solar-Terrestrial Physics Program, Geophys. Monogr. Ser., v.104,* edited by J. L. Horwitz, D. L. Gallagher, and W. K. Peterson, p.371, AGU, Washington, D. C., 1998.

Tsyganenko, N. A., and A. V. Usmanov, Determination of the magnetospheric current system parameters and development of experimental geomagnetic field models based on data from IMP and HEOS satellites, *Planet. Space Sci., 30,* 985, 1982.

Tsyganenko, N. A., S. B. P. Karlsson, S. Kokubun, T. Yamamoto, A. J. Lazarus, K. W. Ogilvie, and C. T. Russell, Global configuration of the magnetotail current sheet as derived from Geotail, Wind, IMP 8, and ISEE 1/2 data, *J. Geophys. Res., 103,* 6827, 1998.

Tsyganenko, N. A., G. Le, C. T. Russell, and T. Iyemori, A study of the inner magnetosphere, based on data of Polar, *J. Geophys. Res., 104,* 10,275, 1999.

Valdivia, J. A., A. S. Sharma, and K. Papadopoulos, Prediction of magnetic storms by nonlinear models, *Geophys. Res. Lett., 23,* 2899, 1997.

Yamamoto, T., K. Shiokawa, and S. Kokubun, Magnetic field structures of the magnetotail as observed by Geotail, *Geophys. Res. Lett., 21,* 2875, 1994.

N. A. Tsyganenko, Code 690.2, Laboratory for Extraterrestrial Physics, NASA Goddard Space Flight Center, Greenbelt, MD 20771. (kolya@nssdca.gsfc.nasa.gov)

(Received October 5, 1999; revised November 18, 1999; accepted November 29, 1999.)